

Fe₃O₄/GRAPHENE OXIDE COMPOSITE FOR ADSORPTION OF METHYLENE BLUE AND METHYL ORANGE IN WATER TREATMENT

M. Khajeh*, A. Barkhordar

Department of Chemistry, University of Zabol, Zabol, Iran;
e-mail: m_khajeh@uoz.ac.ir

Magnetic nanoparticle-graphene oxide (Fe₃O₄/GO) nanocomposite was synthesized for two reasons: this is a good adsorbent for the adsorption of methylene blue (MB) and methyl orange (MO) from aqueous solutions; and due to its magnetic properties, it can be easily separated from aqueous solution using a magnet. This adsorbent was characterized by FTIR, SEM, and XRD techniques. Several parameters such as pH of the solution, the amount of adsorbent, adsorption time, type and volume of elution solvent, and desorption time were optimized to improve the adsorption recovery. The maximum adsorption recovery was obtained at the optimized solution pH of 6.0 using 10.0 mg adsorbent for 10.0 min. According to the Langmuir isotherm, the maximum adsorption capacity was 666.7 and 714.3 mg/g for MB and MO, respectively. The limit of detection (LOD) was also determined as 0.9 and 1.0 µg/L for MB and MO, respectively. Owing to the good repeatability and reproducibility of this adsorbent, it can be considered as a promising candidate for water treatment purposes. Consequently, this adsorbent was used for the adsorption of MB and MO from natural water samples.

Keywords: magnetic nanoparticles, graphene oxide, methylene blue, methyl orange, water samples.

КОМПОЗИТ Fe₃O₄/ОКСИД ГРАФЕНА ДЛЯ АДсорбЦИИ МЕТИЛЕНОВОГО СИНЕГО И МЕТИЛОВОГО ОРАНЖЕВОГО ПРИ ВОДООЧИСТКЕ

M. Khajeh*, A. Barkhordar

УДК 543.42;620.3

Университет Забола, Забол, Иран; e-mail: m_khajeh@uoz.ac.ir

(Поступила 13 марта 2019)

Синтезирован нанокомпозит, состоящий из магнитных наночастиц и оксида графена (Fe₃O₄/GO), который является хорошим адсорбентом метиленового синего (МВ) и метилового оранжевого (МО) из водных растворов и благодаря своим магнитным свойствам легко отделяется от водного раствора с помощью магнита. Адсорбент охарактеризован методами ИК-Фурье-спектроскопии, сканирующей электронной спектроскопии и дифракции рентгеновских лучей. Некоторые параметры (рН раствора, количество адсорбента, время адсорбции, тип и объем элюиционного растворителя, а также время десорбции) оптимизированы для улучшения восстановления адсорбции. Максимальное восстановление адсорбции получено при оптимизированном рН раствора 6.0 с использованием 10.0 мг адсорбента в течение 10 мин. Согласно изотерме Ленгмюра, максимальная адсорбционная способность 666.7 и 714.3 мг/г для МВ и МО. Пределы обнаружения 0.9 и 1.0 мкг/л для МВ и МО. Хорошая повторяемость и воспроизводимость результатов позволяет рассматривать данный адсорбент как перспективный для очистки воды и использовать его для адсорбции МВ и МО из образцов природной воды.

Ключевые слова: магнитные наночастицы, оксид графена, метиленовый синий, метиловый оранжевый, пробы воды.

Introduction. Nowadays, the toxicity of polluted water is mainly due to different synthetic dyes released by the printing, textile, and metallurgy industries [1–3]. The dye industries account for about 20% of all water contamination [4]. The pollution of ground and surface water with synthetic dyes is a serious environmental problem. Dye materials in the effluent of industries are known to be mutagenic, toxic, and car-

cinogenic [5]. For example, methyl orange (MO) and methylene blue (MB), which are used in wool, silk, and cotton [6, 7], can cause various complications, such as nausea, vomiting, and difficulty in breathing [8]. These compounds are nonbiodegradable and highly resistant to oxidizing agents and light. Due to their chemical stability, their removal is a difficult task [9]. In this regard, it is important to develop efficient procedures to remove dyes, such as MO and MB, from environmental water.

Several biological, chemical, and physical methods have been employed to clean up environmental water from these substances [1, 10] among which the adsorption procedure has been widely employed as a promising way due to its low cost, ease of operation, and high removal efficiency [4, 11]. Different traditional adsorbents such as biomaterial, inorganic material, and activated carbon have been applied for the removal of these compounds. However, these sorbents suffer from several disadvantages such as low efficiency and adsorption capacity due to their few active sites, narrow pore diameter, and low surface area [1, 4]. In this context, numerous studies have focused on developing easily renewable and recoverable adsorbents.

To overcome the weaknesses of traditional adsorbents, graphene oxide (GO) can be used. GO is a two-dimensional nanomaterial possessing different hydroxyl, carboxylic acid, and epoxide groups. These functional groups can be helpful in the adsorption of pollutants from environmental waters. Unfortunately, the separation of GO from aqueous samples is difficult. Thus, it has to be functionalized or combined with other materials [1, 12]. Magnetic nanoparticles have been also used in several experiments [13, 14]. The composite of magnetic nanoparticles-GO with magnetic properties could be easily separated from liquid-solid samples using an external magnetic field without tedious centrifugation or filtration [12]. Magnetic reprocessing efficiency will prevent nanoparticle adsorbents from flowing into the natural system and causing unknown damages to the environment.

In the present study, Fe₃O₄/GO composite nanoparticles were synthesized for adsorption and determination of MO and MB from aqueous samples. This sorbent has a large specific surface area for the removal of analytes.

Experimental section. Materials and chemicals. All the chemicals used in this work were of analytical purity and employed without further purification. Methylene blue, methyl orange, ethanol, methanol, FeCl₃ · 6H₂O, FeCl₂ · 6H₂O, and HCl were purchased from Merck (Darmstadt, Germany). A stock standard solution (1000 mg/L) of MB and MO was prepared in double-distilled water, and the working solutions were prepared daily.

Instrumentation. The MO and MB adsorptions were measured by UV-Vis spectrophotometer (UV-2100 RAY Leigh, Beijing, China) at 466 and 644 nm, respectively. The morphology of adsorbent was characterized by scanning electron microscopy (SEM, MIRA3, TESCAN, Czech Republic). X-ray diffraction (XRD) pattern was also obtained using a Philips X'pert diffractometer (Netherlands) employing CuK_α radiation. Fourier transform infrared spectroscopy (FTIR) was carried out in the range 4000 to 500 cm⁻¹ by KBr pellets using Perkin Elmer Spectrum FTIR Version 10.01.00 (USA). The pH of solutions was determined by a Metrohm pH meter (model 630).

Synthesis of Fe₃O₄/GO. The GO was synthesized from purified natural graphite powder using a modified Hummer's method [15, 16]. Co-precipitation and pyrolysis methods were combined to prepare GO/Fe₃O₄ hybrids as proposed in the literature [17, 18]. In a typical process, 450 mg of FeCl₂ · 6H₂O and 120 mg of FeCl₃ · 6H₂O were dissolved in 10 mL of hot diethylene glycol (DEG) in an oil bath at 90°C. Next, the mixture was stirred for 30 min and 2.5 mL of diethanolamine (DEA) was added. Then, the mixture of 6 mmol of NaOH and 5 mL of hot DEG was added to the prepared sample and stirred for 10 min. Afterwards, 15 mg of GO and 10 mL of DEG were mixed and homogenized under vigorous stirring and added to the above mentioned mixture. This mixture was then heated to 180°C in a 50 mL Teflon-lined autoclave. Finally, the mixture was separated by centrifugation, washed several times with ethanol and water, and dried under vacuum. Fe₃O₄/GO is usually formed by *in situ* reduction of iron salt precursor. The magnetic nanoparticles were assembled on the GO surface.

Procedure. Batch dispersive solid phase extraction (DSPE) was employed to optimize various factors. The experiments were performed in a 25 mL flask, where an appropriate amount of adsorbent was added to 25 mL of MB and MO (1 mg/L) sample solution. Next, the pH of aqueous solutions was adjusted by 0.1 mol/L HCl and NaOH. Then, the aqueous phase was stirred for a suitable amount of time at ambient temperature to adsorb the analytes. After that, the adsorbents were separated from the aqueous phase by a magnetic field. The adsorbents will collect at the bottom of the flask due to the strong magnetic field. Finally, the residual concentrations of analytes in the aqueous phase could be determined by a UV-Vis spectrophotometer.

The adsorption recovery (AR%) and adsorption capacity (q_e) can be calculated by the following equations:

$$\text{AR}\% = \frac{C_0 - C_e}{C_0} \times 100,$$

$$q_e = \frac{(C_0 - C_e)V}{M},$$

where C_0 and C_e (mg/L) are the initial and equilibrium concentrations of the analytes in the aqueous, respectively, q_e (mg/g) denotes the adsorption capacity of adsorbent at equilibrium time, M (g) represents the adsorbent mass, and V (L) is the volume of the analyte solution.

For the desorption of analytes, methanol, ethanol, and acetonitrile were used as the eluent solvents. The appropriate volume of the eluent solvent was mixed with analyte-loaded adsorbent and shaken for a suitable amount of time at ambient temperature. Then, the adsorbent was magnetically separated for the eluent solvent. Finally, the analyte concentrations in the eluent solvent were determined by UV-Vis spectrophotometry.

Results and discussion. Characterization. Figure 1 shows the FTIR spectra of adsorbent in the range 500–4000 cm^{-1} . The band at 590 cm^{-1} belongs to the Fe-O stretching vibration of Fe_3O_4 in the adsorbent. The peak at 1714 cm^{-1} is attributed to C=O band of the carboxyl group. Moreover, the peaks corresponding to stretching vibration of C-O, C-OH, and C=C can be observed at 1084, 1365, and 1625 cm^{-1} , respectively. The broad band at 3421 cm^{-1} is related to O-H stretching vibration [1, 10]. This figure confirms the successful preparation of $\text{Fe}_3\text{O}_4/\text{GO}$ adsorbent. All the functional groups served as adsorption sites and played an essential role in the adsorption of MB and MO from the sample solutions.

Figure 2 shows the XRD patterns of the $\text{Fe}_3\text{O}_4/\text{GO}$ nanocomposite in the investigation of the crystalline structure of the adsorbent. The diffraction peaks at $2\theta = 30.05, 35.5, 43.1, 53.4,$ and 57.3° correspond to the (220), (311), (400), (422), and (551) planes of adsorbent, respectively.

SEM images at various magnifications are depicted in Fig. 3. As can be seen, the adsorbent presents a uniform spherical morphology with a size range of 78–110 nm.

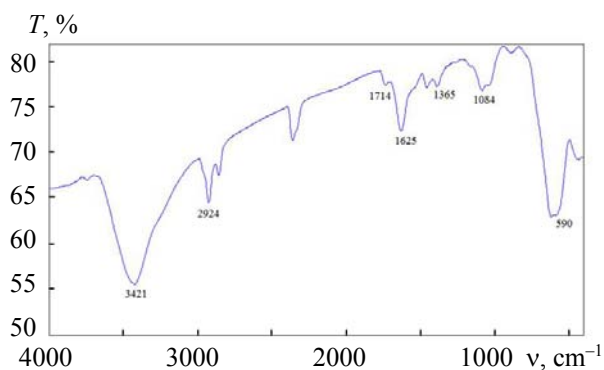


Fig. 1. FTIR spectra of the adsorbent.

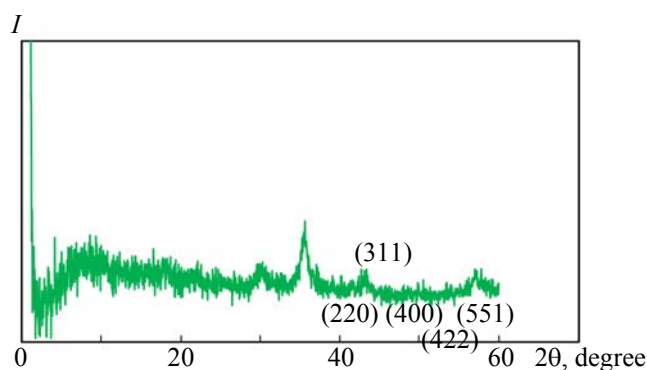


Fig. 2. XRD patterns of the adsorbent.

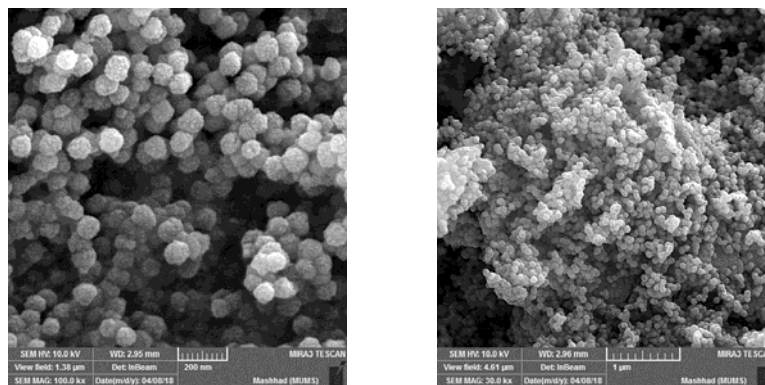


Fig. 3. SEM images of adsorbent.

Factors affecting the adsorption efficiency. The pH can influence the charge transfer on the liquid/solid interface and hence affect the adsorption of the analyte from the sample solutions. Figure 4a indicates the effect of pH (in the range of 3.0–8.0) on the adsorption recovery. The maximum adsorptions for both analytes were obtained at pH 6.0. The high adsorption of the analytes by the adsorbent surface can be due to electrostatic attraction between the adsorbent surface and the analytes. Similar behavior has been reported in the literature [19, 20]. As a result, pH of 6.0 was used in the subsequent experiments.

The effect of the sorbent amount (2.0 to 30.0 mg) on the adsorption recovery of MO and MB was studied by adding various amounts of nanocomposite into the sample solutions. Figure 4b reveals the effect of the amount of adsorbent on the adsorption recovery of both analytes. According to this figure, the recovery is increased by raising the amount of adsorbent. The amount of adsorbent determines the contact area between the analytes and the adsorbent. Upon increase in the amount of adsorbent, additional adsorption sites will be available; hence the adsorption will be enhanced. However, when the extraction of the analytes reaches a saturated state, further increase in the amount of adsorbent does not result in further increase in the MB and MO extraction. Therefore, an increase in the amount of adsorbent will only produce more waste. The highest recovery was obtained using 10.0 g of adsorbent. Therefore, 10.0 mg of adsorbent was used in subsequent experiments.

The adsorption time (2.0 to 20.0 min) is an essential factor in the adsorption procedure of Fe₃O₄/GO composite. The effect of adsorption time on the adsorption recovery is depicted in Fig. 4c. The results demonstrate that the adsorption of both analytes increased initially with enhancement in the adsorption time as more active adsorption sites will be available on the adsorbent. The adsorption recovery finally tended to a constant value due to the decrease in the number of accessible active adsorption sites. In the subsequent experiments, 10.0 min of adsorption time was used.

Adsorption and desorption processes can be employed to study the reusability of the adsorbent. It is also essential to determine which adsorbent can be easily regenerated and which desorbing agent (eluent solvent) is inexpensive, nonpolluting, and effective and causes no damage to the adsorbent structure [21]. The adsorbent was washed with various eluents such as methanol, ethanol, and acetonitrile to desorb the adsorbent. The best adsorption recovery was achieved by ethanol. Then the desorption volume and time were evaluated. After separation of the adsorbent from aqueous solution, it was mixed with different volumes of ethanol (0.2–1.0 mL), and the sample solution was stirring for 2.0 to 15.0 min. According to the results, 0.5 mL and 5.0 min were selected as optimal eluent volume and desorption time, respectively.

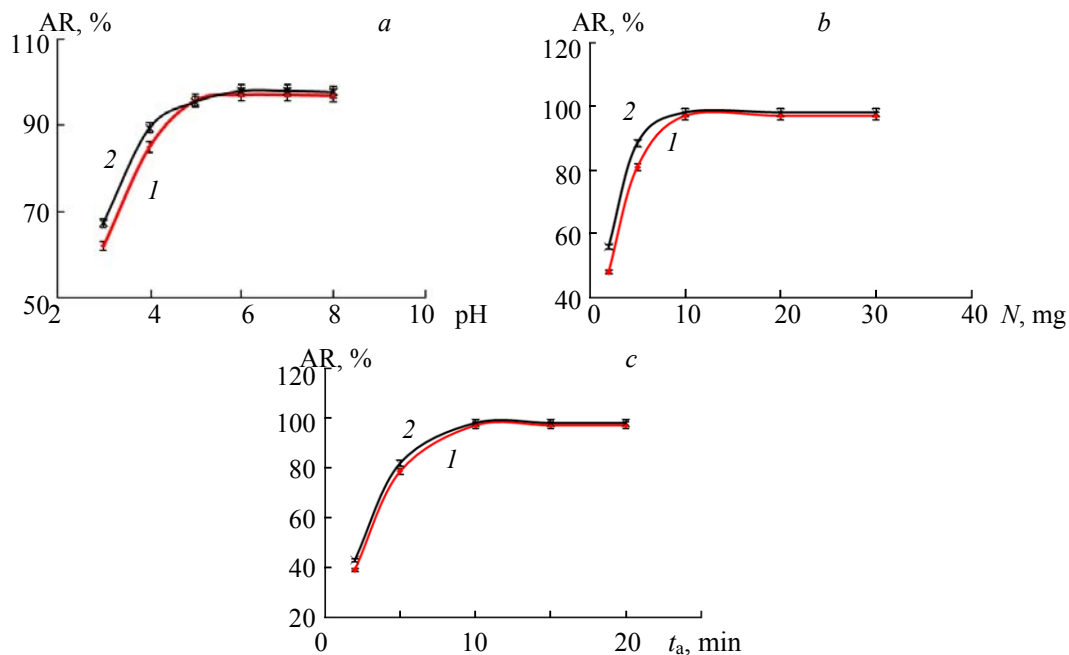


Fig. 4. a) The effect of pH on the adsorption recovery of MO (1) and MB (2) (adsorption time 10 min and amount of adsorbent 10.0 mg), b) The effect of amount of adsorbent (N) on the adsorption recovery (adsorption time 10 min and pH 6.0), c) The effect of adsorption time (t_a) on the adsorption recovery (pH 6.0 and amount of adsorbent 10.0 mg).

The reusability of the adsorbent is shown in Fig. 5. Based on this figure, after six cycles, the adsorbent still exhibited a proper adsorption recovery.

The adsorption procedure can continue until the adsorbent and adsorbate reach dynamic equilibrium. The adsorption isotherms describe the relationship between the adsorbate and surface of the adsorbent. Figure 6 shows the adsorption of MO and MB on the Fe₃O₄/GO at various initial concentrations. The equilibrium adsorption data were fitted by the Freundlich and Langmuir models [22]. The Langmuir adsorption isotherm equation was used to fit monolayer sorption as follows:

$$\frac{C_e}{q_e} = \frac{1}{q_m K_L} + \frac{C_e}{q_m},$$

where C_e is the adsorbate equilibrium concentration (mg/L); K_L denotes the Langmuir constant (L/mg); q_e represents the amount of adsorbed analyte per unit mass of the adsorbent, and q_m is the maximum adsorption capacity (mg/g).

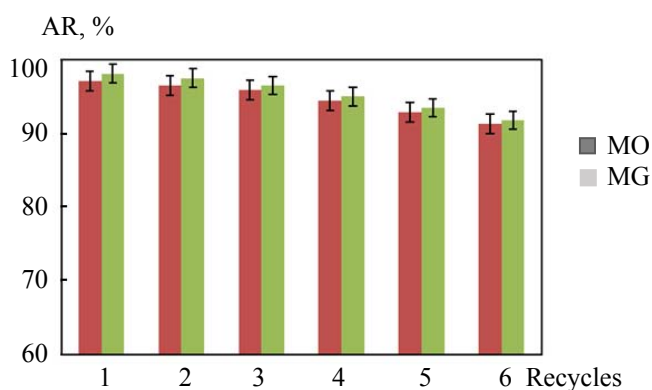


Fig. 5. Adsorption-desorption recycles.

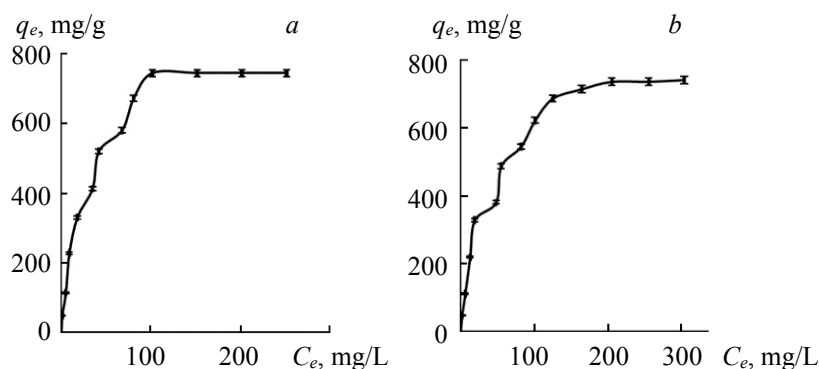


Fig. 6. Adsorption isotherms of MB (a) and MO (b) on the adsorbent.

The Freundlich model can be employed for heterogeneous surfaces and multilayer adsorption. The Freundlich adsorption isotherm equation used to fit the heterogeneous sorption has the following form:

$$\ln q_e = \ln K_F + (1/n) \ln C_e,$$

where $1/n$ is the adsorption intensity, and K_F stands for the Freundlich constant related to adsorption capacity.

Table 1 lists the effective factors (n , K_F , K_L , and q_m) of the adsorption models as well as the determination coefficient (R^2). The results showed that the Langmuir model fit well the experimental data in the studied range as its R^2 value was higher than that of the Freundlich model for both analytes. This phenomenon can be attributed to the homogenous distribution of active sites on the adsorbent surface. The adsorption increase can be also assigned to the values of n in the range of 1 to 10 [23]. In the present study, the values of n were in the mentioned range for both analytes, suggesting favorable adsorption.

TABLE 1. Regression Parameters of Adsorption Isotherms of MO and MB onto Adsorbent Fitted by Langmuir and Freundlich Models

Pollutants	Langmuir model			Freundlich model		
	q_m (mg/g)	k_L (L/mg)	R^2	K_F (mg/g)/(mg/L) ^{1/n}	n	R^2
MB	666.7	0.076	0.9963	63.62	2.03	0.9326
MO	714.3	0.037	0.9932	46.98	1.87	0.9427

The separation factor (R_L) for the adsorption of both analytes on the adsorbent surface was calculated by the equation $R_L = 1/(1+KC_0)$, where C_0 is the initial concentration of both analytes and K_L (L/mg) represents the Langmuir constant. The R_L value determines the isotherm shapes, such that $R_L > 1$, $R_L = 1$, $0 < R_L < 1$, and $R_L = 0$ are indicative of unfavorable, linear, favorable, and irreversible adsorption, respectively [24]. For both analytes, the value of R_L was < 1 , showing favorable adsorption.

Performance evaluation. To determine the performance, various concentrations of both analyte were prepared, and adsorption was carried out by the DSPE method. Under the optimized condition, the calibration curve was constructed to assess the linearity between adsorption recovery and concentration of both analytes. The calibration curve for both analytes was linear in the range 0.01–3.0 mg/L, with correlation coefficients (R^2) of 0.996 and 0.994 for MB and MO, respectively. The limits of detection (LOD) were also determined as 0.9 and 1.0 $\mu\text{g/L}$ for MB and MO, respectively (LOD = $3S_d/m$, where S_d and m are the blank standard deviation and the slope of the calibration curve, respectively). The precision was shown as the relative standard deviation (RSD%). The intra-day and inter-day precisions ($n = 5$, $c = 50.0 \mu\text{g/L}$) were 2.8, 3.1% (intra-day) and 1.4 and 1.3% (inter-day) for MO and MB, respectively.

The maximum adsorption capacity (mg/g) of Fe₃O₄/GO sorbent is compared with the previously-reported adsorbents for MB and MO adsorption in Table 2. As can be seen, Fe₃O₄/GO has promising potential for adsorption of methyl orange and methylene blue from the aqueous solution.

TABLE 2. Comparison of the Present Method with Previous Methods for Extraction of MB and MO

Adsorbent	Maximum adsorption capacity (mg/g)		Reference
	MB	MO	
Sulfonated graphene aerogel	660.0	–	[25]
Fe ₃ O ₄ /ppy/RGO	270.3	–	[26]
Montmorillonite nanosheets/chitosan hydrogels	538.0	–	[27]
CuO nanoparticles	–	370.3	[28]
Grapheme oxide	–	686.89	[5]
Grapheme oxide	–	16.83	[10]
Fe ₃ O ₄ /Go nanocomposite	666.7	714.3	This work

Real samples. The applicability of the above procedure to the adsorption of MB and MO was tested in natural water samples. These samples were collected from Chah-e Nimeh (Zabol, Iran, Chah-e Nimeh reservoirs are three big and natural cavities in Zabol). It contains 50 million square meters of water and is used to provide drinking water to Zabol City. No MB and MO were detected in these samples. Therefore, the real samples were spiked with different amounts of both analytes (Table 3). The results indicated that the proposed procedure can be successfully employed for the adsorption of both analytes (Table 3). Moreover, the results concerning seawater (which contains different salts) showed that the presence of other salts does not affect the analyte extraction.

TABLE 3. Determination of MB and MO in Water Samples

No. Sample	Added ($\mu\text{g/L}$)	Found ($\pm^a\text{RSD}\%$)		AR%	
		MB	MO	MB	MO
1	50.0	49.1 (± 0.9)	48.9 (± 1.4)	98.2	97.8
	100.0	98.0 (± 1.1)	98.2 (± 1.2)	98.0	98.2
2	50.0	48.8 (± 1.0)	48.5 (± 0.8)	97.6	97.0
	100.0	98.6 (± 1.3)	97.5 (± 1.0)	98.6	97.5

^a Relative standard deviation.

Conclusions. Fe₃O₄/Go nanocomposite was synthesized and used for the adsorption of MB and MO from the aqueous sample solution. This adsorbent was highly effective for MB and MO. The optimized values of pH, adsorbent amount, and adsorption time were found to be 6.0, 10.0 mg, and 10.0 min, respectively. The adsorption equilibrium data for both analytes were obtained by two types of isotherms, including the Langmuir and Freundlich models. The determination coefficient of Langmuir was higher than that of Freundlich. The maximum adsorption (q_m) for MB and MO were 666.7 and 714.3 mg/g, respectively. The results indicated that, compared to the other adsorbents, the proposed adsorbent has higher adsorption capacity and a faster adsorption rate for MB and MO. The adsorbent can be also recycled six times while maintaining good reproducibility, which can reduce the costs. This adsorbent exhibited good applicability for the adsorption of dyes from natural water samples.

Acknowledgments. The University of Zabol is gratefully acknowledged for financial support of this work (Grant number: UOZ-GR-9517-1).

REFERENCES

1. M. P. Wei, H. Chai, Y. L. Cao, D. Z. Jia, *J. Colloid Interf. Sci.*, **524**, 297–305 (2018).
2. Y. Wu, M. Xu, X. Chen, S. Yang, H. Wu, J. Pan, X. Xiong, *Nanoscale*, **8**, 440–450 (2016).
3. M. Khajeh, A. R. Golzary, *Spectrochim. Acta A: Mol. Biomol. Spectrosc.*, **131**, 189–194 (2014).
4. P. Zhang, I. Lo, D. OConnor, S. Pehkonen, H. Cheng, D. Hou, *J. Colloid Interf. Sci.*, **508**, 39–48 (2017).
5. Y. Wang, G. Xia, C. Wu, J. Sun, R. Song, W. Huang, *Carbohydr. Polym.*, **115**, 686–693 (2015).
6. S. C. Nunez, T. M. Yoshimura, M. S. Ribeiro, H. C. Junqueira, C. Maciel, M. D. Coutinho-Neto, M. S. Baptista, *J. Photochem. Photobiol. B*, **150**, 31–37 (2015).
7. R. Gong, J. Ye, W. Dai, X. Yan, J. Hu, X. Hu, Sh. Li, H. Huang, *Ind. Eng. Chem. Res.*, **52**, 14297–14303 (2013).
8. W. Stawinski, A. Wegrzyn, T. Danko, O. Freitas, S. Figueiredo, L. Chemielarz, *Chemosphere*, **173**, 107–115 (2017).
9. Z. Xiao, Q. Zhou, H. Qin, J. Qiao, X. Guan, *Desalin. Water Treat.*, **57**, 1659–1670 (2016).
10. D. Robati, B. Miza, M. Rajabi, O. Moradi, I. Tyagi, S. Agarwal, V. K. Gupta, *Chem. Eng. J.*, **284**, 687–697 (2017).
11. R. Chen, W. Wang, X. Zhao, Y. Zhang, S. Wu, F. Li, *Chem. Eng. J.*, **242**, 226–233 (2014).
12. L. Cui, Y. Wang, L. Gao, L. Hu, L. Yan, Q. Wei, B. Du, *Chem. Eng. J.*, **281**, 1–10 (2015).
13. X. Gao, X. Yao, Z. Zhong, L. Jia, *Talanta*, **186**, 147–153 (2018).
14. M. Khajeh, E. Sanchooli, *J. Food Compos. Anal.*, **23**, 677–680 (2010).
15. X. Sun, Z. Liu, K. Welsher, J. T. Robinson, A. Goodwin, S. Zaric, H. Dai, *Nano Res.*, **1**, N 3, 203–212 (2008).
16. C. Zhou, H. Wua, M. Wang, C. Huang, D. Yang, N. Jia, *Mater. Sci. Eng. C*, **78**, 817–825 (2017).
17. L. Yu, H. Wu, B. Wu, Z. Wang, H. Cao, C. Fu, N. Jia, *Nano-Micro Lett.*, **6**, 258–267 (2014).
18. H. Wu, G. Liu, Y. Zhuang, D. Wu, H. Zhang, H. Yang, H. Hu, S. Yang, *Biomaterials*, **32**, N 21, 4867–4876 (2011).
19. R. Gong, J. Ye, W. Dai, X. Yan, J. Hu, X. Hu, S. Li, H. Huang, *Ind. Eng. Chem. Res.*; doi: 10.1021/ie402138w.
20. L. Ai, C. Zhang, L. Meng, *J. Chem. Eng. Data*, **56**, 4217–4225 (2011).
21. D. Kołodyn'ska, J. Krukowska, P. Thomas, *Chem. Eng. J.*, **307**, 353–363 (2017).
22. Q. F. Yao, Y. Xiong, H. W. Wang, C. Wang, Q. F. Sun, *J. Mater. Chem. A*, **5**, 9580–9590 (2017).
23. M. Khajeh, A. Sarafraz-Yazdi, A. Fakhr Rai Moghadam, *Arab. J. Chem.*, **10**, S1663–S1673 (2017).
24. H. Li, D. Xiao, H. He, R. Lin, P. Zuo, *Trans. Nonferrous Mater. Soc. China*, **23**, 2657–2665 (2013).
25. S. Scalsese, I. Nicotera, D. Dangelo, S. Filice, S. Libertino, C. Simari, K. Dimosd, V. Privitera, *New J. Chem.*, **40**, 3654–3663 (2016).
26. I. Z. Bai, Z. P. Li, Y. Zhang, T. Wang, R. H. Lu, W. F. Zhou, H. X. Gao, S. B. Zhang, *Chem. Eng. J.*, **279**, 757–766 (2015).
27. S. Kang, Y. Zhao, W. Wang, T. Zhang, T. Chen, H. Yi, F. Rao, S. Song, *Appl. Surf. Sci.*, **448**, 203–211 (2018).
28. A. A. A. Darwish, M. Rashad, Hatem A. Al-Aoh, *Dyes Pigments*, **160**, 563–571 (2019).